Agrobacteria reprogram virulence gene expression by controlled release of host-conjugated signals

Chao Wang[a,b,1], Fuzhou Ye[c,1], Changqing Chang[a,1], Xiaoling Liu[b,d], Jianhe Wang[a], Jinpei Wang[a], Xin-Fu Yan[c], Qinqin Fu[c], Jianuan Zhou[a], Shaohua Chen[a], Yong-Gui Gao[b,c,2], and Lian-Hui Zhang[a,b,2]

[a]Guangdong Province Key Laboratory of Microbial Signals and Disease Control, Integrative Microbiology Research Centre, South China Agricultural University, 510642 Guangzhou, China; [b]Institute of Molecular and Cell Biology, 138673, Singapore; [c]School of Biological Sciences, Nanyang Technological University, 637551, Singapore; and [d]Chongqing Academy of Chinese Materia Medica, Chongqing City, 400065, China

Edited by P. Zambryski, University of California, Berkeley, CA, and approved September 18, 2019 (received for review March 4, 2019)

It is highly intriguing how bacterial pathogens can quickly shut down energy-costly infection machinery once successful infection is established. This study depicts that mutation of repressor SghR increases the expression of hydrolase SghA in *Agrobacterium tumefaciens*, which releases plant defense signal salicylic acid (SA) from its storage form SA β-glucoside (SAG). Addition of SA substantially reduces gene expression of bacterial virulence. Bacterial *vir* genes and *sghA* are differentially transcribed at early and later infection stages, respectively. Plant metabolite sucrose is a signal ligand that inactivates SghR and consequently induces *sghA* expression. Disruption of *sghA* leads to increased *vir* expression *in planta* and enhances tumor formation whereas mutation of *sghR* decreases *vir* expression and tumor formation. These results depict a remarkable mechanism by which *A. tumefaciens* taps on the reserved pool of plant signal SA to reprogram its virulence upon establishment of infection.

chemical signaling | cost–pathogen interaction | *Agrobacterium* | sucrose | glucosidase

Bacterial pathogens commonly deploy an array of virulence factors to establish infections in various host organisms. For example, major virulence genes of *Agrobacterium tumefaciens* are carried by a large plasmid (over 200 kb), and infection requires a range of regulatory and structural proteins and a DNA fragment, which are transported from bacterial cells into host plant cells (1). These virulence factors are energy-costly to synthesize, and therefore bacteria might have evolved mechanisms to reprogram expression of virulence genes to survive in changed environmental conditions. *Pseudomonas aeruginosa* is known to switch from acute infection to chronic persistence by turning off expression of the genes encoding the type III secretion system (T3SS) through the Gac/Rsm regulatory pathway at the later stage of infection (2). Contrarily, *Salmonella enterica* escapes from its intracellular niche and spreads to a secondary infection site by inducing the expression of invasion-associated T3SS genes (3). However, how bacterial pathogens sense and perceive environmental changes to reprogram virulence gene expression remains elusive.

A. tumefaciens is a renowned plant pathogen for causing crown gall diseases on more than 140 plant species (4). Infection of agrobacteria is modulated by various plant-derived chemical signals (5). Initially, wound-associated acidic conditions induce the expression of the chromosomal ChvG/I 2-component system, which activates the expression of transcriptional regulator VirG. VirA senses acetosyringone in the wounding site, phosphorylates VirG, and activates the expression of *vir* regulon that encodes the type IV secretion system and accessory proteins for processing and transferring transfer DNA (T-DNA) into plant cells. After integration, T-DNA genes encode biosynthesis of auxin, cytokinin, and opines. Plant hormones auxin and cytokinin promote plant cell proliferation and formation of crown gall tumors whereas opines are utilized by *A. tumefaciens* as specific nutrients. The bacterial pathogen thus creates an ecological niche that provides a selective advantage over other bacterial species, and this phenomenon is known as genetic colonization (6).

Transformation of host plant cells and building up of competitive advantages in ecological systems make *A. tumefaciens* an excellent model for exploring various features of pathogen–host interactions (7). *A. tumefaciens* infection is sensitive to high temperature, and therefore crown gall disease rarely happens in tropical regions. Previous findings suggest that *Agrobacterium*-mediated infection requires only a short period of time (8). This raises an intriguing question how pathogen can turn down *vir* expression after the infection to reduce energy cost. In this regard, it is interesting to note that exogenous application of plant defense signal salicylic acid (SA) can inhibit *vir* gene expression and virulence of *A. tumefaciens* (9, 10). In plants, a proportion of SA conjugates with glucose to prepare the storage form SA β-glucoside (SAG) (11, 12). Thus, it would be fascinating to explore if *Agrobacterium* has evolved a mechanism to hijack SA of host plants to switch from infection mode to free living style after the initiation of crown gall formation.

In this study, we report identification and characterization of a gene, *sghA*, encoding a hydrolytic enzyme. This enzyme releases

Significance

Bacterial infection has been extensively investigated; however, little is known about how bacterial pathogens timely shut down infecting machinery after successful infections. Here, a previously unknown sucrose–SghR/SghA–SAG–SA signaling axis was identified which controls the timing to shut off bacterial virulence expression and fine-tune host immune response. Sucrose, salicylic acid (SA), and its storage form SAG are small chemicals produced in plants whereas SghR is a bacterial sensor of sucrose and SghA is a bacterial enzyme that releases SA from SAG. Given that SA is an imperative signaling molecule in defense against a variety of microbial pathogens, these results depict a previously unknown 2-way chemical signaling cross-talk during microbe–host coevolution and shed mechanistic insights into host–bacteria interaction.

Author contributions: C.W., Y.-G.G., and L.-H.Z. designed research; C.W., F.Y., C.C., X.L., Jianhe Wang, Jinpei Wang, X.-F.Y., Q.F., J.Z., and S.C. performed research; L.-H.Z. contributed new reagents/analytic tools; C.W., F.Y., Y.-G.G., and L.-H.Z. analyzed data; and C.W., Y.-G.G., and L.-H.Z. wrote the paper.

The authors declare no competing interest.

This article is a PNAS Direct Submission.

Data deposition: Atomic coordinates and structural factors have been deposited in the Protein Data Bank, www.wwpdb.org (PDB ID codes 6RJK [Apo], 6RK2 [with SAG], 6RJO [with salicin], and 6RJM [with glucose]).

[1]C.W., F.Y., and C.C. contributed equally to this work.

[2]To whom correspondence may be addressed. Email: lhzhang01@scau.edu.cn or ygao@ntu.edu.sg.

This article contains supporting information online at www.pnas.org/lookup/suppl/doi:10.1073/pnas.1903695116/-/DCSupplemental.

First published October 11, 2019.

SA from SAG to elevate its levels *in planta*. Transcription of *sghA* is tightly repressed by a repressor (SghR), and plant metabolite sucrose specifically releases this repression. Study further revealed that exogenous addition of SA decreased *vir* gene expression in *A. tumefaciens*. This phenomenon confirmed that the pathogen could use SA to reset its virulence via SghR/SghA after completing their infection. SA is an essential signal molecule for plant local defense and systemic resistance against numerous plant pathogens. These results indicate a broad implication in controlling crown gall disease and increasing plant transformation efficiency in agriculture. This study also unravels a previously unknown sophisticated strategy of microbial infection evolved during the long history of pathogen–host interaction.

Results

Null Mutation of Repressor SghR Increases the β-Galactosidase Activity of *A. tumefaciens*. SAG, a glucose-conjugated salicylic acid in plant hosts, shares a similar structure with 5-bromo-4-chloro-3-indolyl-β-D-galactopyranoside (X-gal) and ortho-nitrophenyl-β-D-galactopyranoside (ONPG) (*SI Appendix*, Fig. S1). This tempted us to search for potential SAG-hydrolyzing enzymes by using agar plates supplemented with X-gal. Wild-type *A. tumefaciens* strain A6 did not show obvious β-galactosidase activity as the color of bacterial colonies remained unchanged in the X-gal plate (Fig. 1*A*). Assuming that the bacterium may contain a repressed gene encoding SAG hydrolytic enzyme, we generated a library of transposon mutants and screened for enhanced β-galactosidase activity. After screening over 20,000 mutants, one mutant was identified that exhibited a dark blue color on basic medium (BM) plates supplemented with X-gal. Sequence analyses showed that Tn5 was inserted in *A. tumefaciens* strain C58 homolog *atu1522* sharing 92% amino acid sequence identity (GenBank no. KU512833). Its translational product is a 350-amino acid (aa) protein containing a helix-turn-helix (HTH)-type DNA-binding domain at its N terminus and a periplasmic binding protein-like domain (Peripla_BP_3) at its C terminus (Fig. 1*B*). These findings suggest that *atu1522* homolog gene might encode a SAG hydrolase gene repressor and was named as *sghR*. Fig. 1*A* shows blue color morphology of *sghR* mutant (*sghR*::Tn5) on an X-gal agar plate. ONPG-based quantitative analysis indicated that *sghR* mutation increased β-galactosidase–like activity by about 10-fold as compared to parental strain A6 (Fig. 1*A*)

To identify the SghR-repressed gene encoding putative SAG hydrolase, another round of mutagenesis was conducted with transposon Mariner by using mutant *sghR*::Tn5 as the parental strain. Screening of the resultant mutant library identified 1 mutant with much reduced blue color on X-gal agar plates than the parental strain. Sequence analysis showed that Mariner was inserted in an ORF sharing about 94% identity to the *atu4485* gene localized on the linear chromosome of *A. tumefaciens* strain C58. Sequence analysis showed that homolog *atu4485* encodes a 467-aa protein (GenBank no. KU512832), and this putative SAG hydrolase gene was designated as *sghA*. An X-gal plate assay showed that disruption of *sghA* by *sghR* mutant abolished its blue color morphology (Fig. 1*A*), suggesting that *sghA* is the sole SghR-repressed gene encoding putative SAG hydrolase. *In trans* expression of *sghA* in double mutant *sghRA*::Tn restored blue color morphology on the X-gal plate and significantly increased β-galactosidase activity against ONPG (Fig. 1*A*). In silico analysis was conducted with the online tool SMART (http://smart.embl-heidelberg.de), and results revealed that SghA contains a glycoside hydrolase family 1 (Glyco_hydro_1) domain (Fig. 1*B*). This is a typical feature of the glycoside hydrolase family comprising numerous enzymes, including β-glucosidase, β-galactosidase, 6-phospho-β-galactosidase, 6-phospho-β-glucosidase, and β-mannosidase.

SghA as SA-Releasing Enzyme. To test whether SghA could hydrolyze SAG to release SA, SAG was synthesized by using a modified

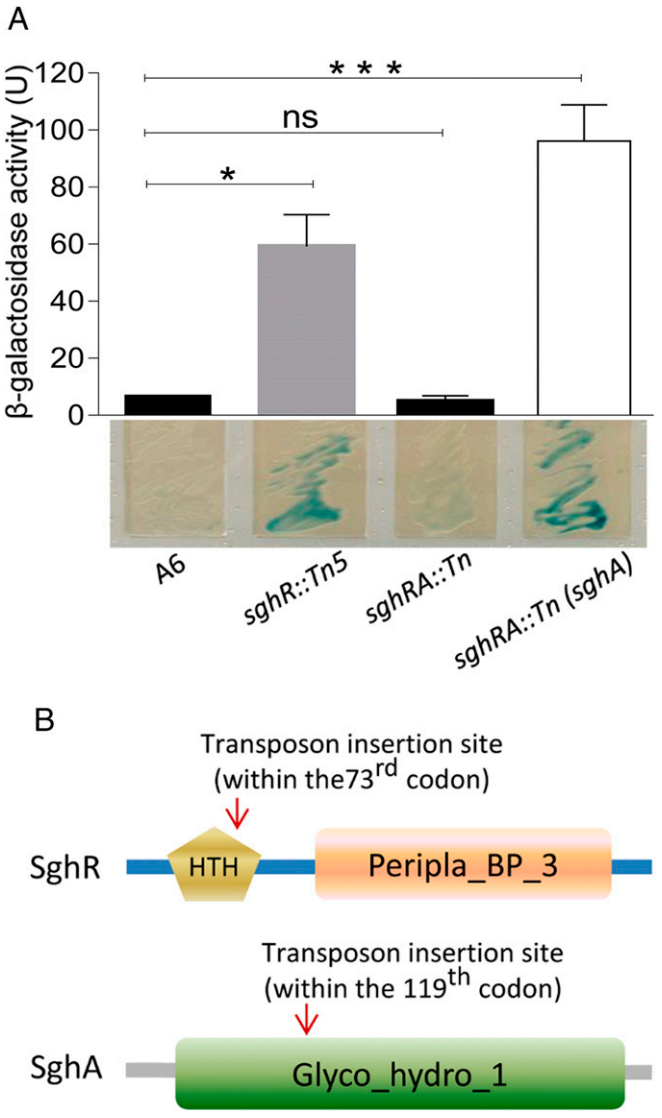

Fig. 1. β-galactosidase activity of *A. tumefaciens* strain A6 and derivatives. (*A*) Analysis of β-galactosidase activity of *A. tumefaciens* A6 and its derivatives in liquid culture (*Top*) and on solid agar plates (*Bottom*). U, Miller Unit. (*B*) Domain structures of SghR and SghA. Glyco_hyddro_1, glycoside hydrolase family 1 domain; HTH, HTH-type DNA binding domain; Peripla_BP_3, periplasmic binding protein-like domain 3. Experiments in *A* were repeated 5 times, and each time in duplicate. A nonparametric Kruskal–Wallis 1-way ANOVA was performed in GraphPad for statistical analyses. Values and error bars represent means and SD. *$P < 0.05$; ***$P < 0.0001$; ns, not significant.

protocol (*SI Appendix*, Fig. S2). After structural verification with mass spectrometry (MS) and NMR, SAG molecules were incubated with recombinant SghA and boiling-denatured SghA, respectively. High performance liquid chromatography (HPLC) analysis of the denatured SghA reaction mixture detected only 1 SAG peak at a retention time of 5.0 min (Fig. 2*A*) and was confirmed by electrospray ionization mass spectrometry (ESI-MS) analysis (*SI Appendix*, Fig. S3*A*). In contrast, HPLC analysis resolved 2 peaks from the reaction mixture of active SghA: i.e., SAG peak at 5 min and a new peak at a retention time of 9.0 min (Fig. 2*A*). ESI-MS analysis of the new peak showed a strong quasimolecular (M-H) ion with an *m/z* of 137.00 (*SI Appendix*, Fig. S3*B*) corresponding to the molecular mass of SA. Glucose, another predicted enzymatic reaction product, was not detected in this HPLC analysis as the molecule lacks detectable UV absorbance.

These results unequivocally demonstrated that SghA is a β-glucosidase that hydrolyzes SAG to release SA.

To determine the enzyme specificity of SghA, its catalytic activity was compared against SAG analogs. Results showed that SghA also hydrolyzed salicin to produce a product peak at around 4.0 min (Fig. 2*B*). ESI-MS analysis of this new peak fraction showed a strong quasimolecular (M-H) ion at an *m*/*z* of 123.00, similar to salicin-hydrolyzed product salicylic alcohol (*SI Appendix*, Fig. S3*C*). However, SghA could not hydrolyze other SAG structural analogs coniferin and sucrose (*SI Appendix*, Fig. S4), indicating the substrate selectivity of SghA. Consistent with this finding, SghA digested SAG at a much faster rate than salicin and ONPG under the same reaction conditions (Fig. 2 *A* and *B*). Michaelis constant (K_m) of SghA was determined as 0.47 mM, 2.81 mM, and 5.91 mM for SAG, salicin, and ONPG, respectively (*SI Appendix*, Fig. S5). SghA of agrobacterium cells in culture in medium readily cleaved exogenous SAG to its metabolic product SA, as detected in the culture supernatant (*SI Appendix*, Fig. S6). These results suggest that SAG entered the bacterial cells and its cleaved product was exported out.

To further understand the molecular bases of SghA substrate specificity and catalytic mechanism, 2 substrates SAG and salicin were used to determine SghA structures in apo and in complex. The apo-SghA structure showed a typical $(\beta/\alpha)_8$-barrel fold in a single domain (*SI Appendix*, Fig. S7*A*), which is commonly found in β-glycoside hydrolase family 1 (GH1). The asymmetric unit contains 2 SghA molecules and forms a homodimer whereas dimerization does not influence the free access to its active site

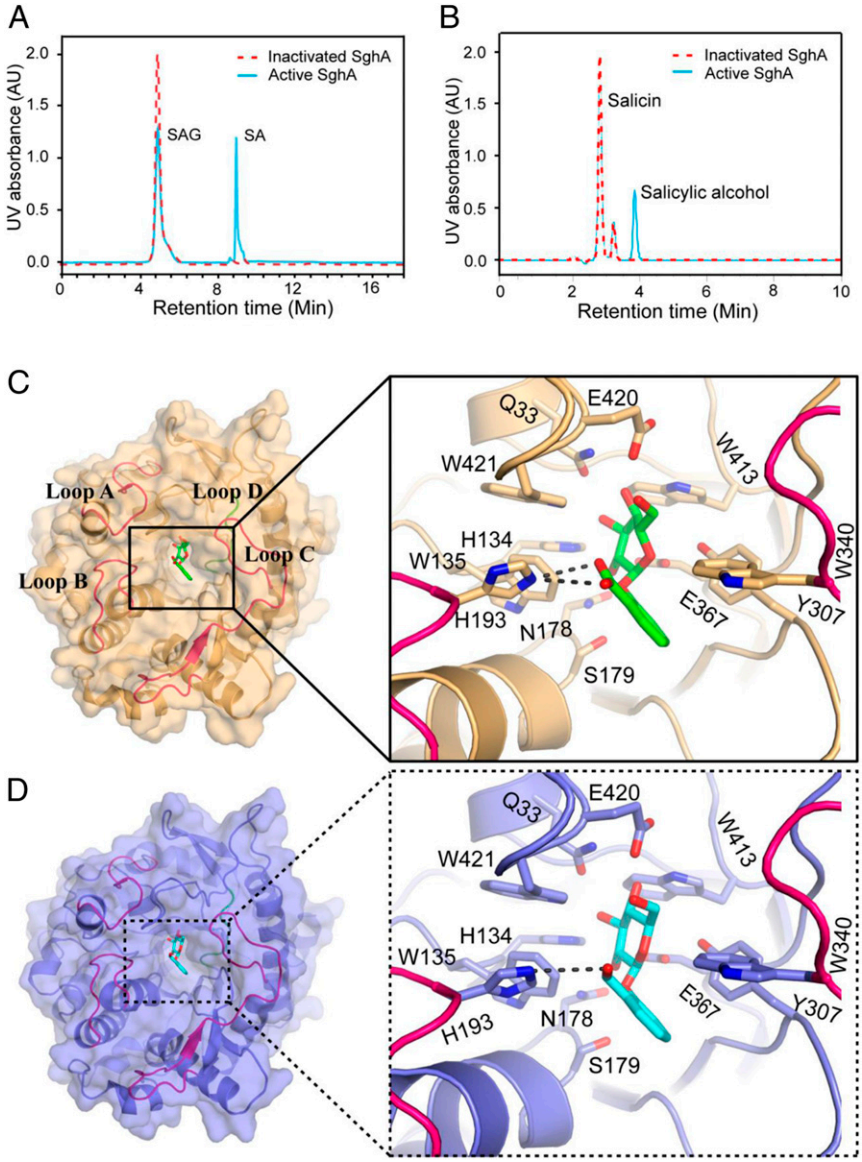

Fig. 2. SghA releases SA from SAG. (*A*) HPLC profile of reaction mixtures containing SAG treated with SghA (blue) and denatured SghA (red). (*B*) HPLC profile of reaction mixtures containing salicin treated with SghA (blue) and denatured SghA (red). HPLC experiments were repeated at least 3 times, and 1 set of representative data is presented. AU, arbitrary unit. (*C*) Catalytic site of SghA in the presence of SAG. SAG is shown as a stick, and carbon and oxygen atoms are colored green and red, respectively. Residues involved in SAG binding are shown as a stick model. Hydrogen bonds between His216 of SghA and SAG are indicated by a dashed line. Loops A to D (residues 54 to 69, 189 to 200, 314 to 344, and 365 to 384, respectively) are colored red and blue (loop D only) (same as in *D*). (*D*) Binding pocket of SghA in the presence of salicin. Salicin is shown as a stick, and carbon and oxygen atoms are colored cyan and red, respectively. Residues interacting with salicin are shown as a stick model. The hydrogen bond between His216 of SghA and salicin is indicated by a dashed line.

(*SI Appendix*, Fig. S7 *B* and *C*). Based on the comparison of the apo-SghA structure with other reported homolog structures, we identified that E179 of SghA plays a critical role in its activity. Substitution of E179 with S179 completely abolished enzymatic activity, as reflected by ONPG hydrolysis.

SghA–SAG and SghA–salicin complexes were cocrystallized by generating a hydrolase-dead mutant SghA(E179S) (*SI Appendix*, Fig. S8). Similar to other GH1 family proteins (13), SghA also has a bell-shaped binding cavity where glycone (sugar) buries inside and aglycone is located at the wide entrance gate (Fig. 2 *C* and *D*). To form the SghA–SAG complex, highly conserved residues (Q33, H134, N178, E367, and E420) formed hydrogen bonds with hydroxyl groups of sugar. Sugar binding was stabilized by the interacting of SAG with Y307 and W413 side chains on one side and indole groups of W135 and W421 from the other. SghA interaction with the aglycone group of SAG involved H193 in loop B and W340 in loop C to form a sandwich arrangement. In particular, 2 hydrogen bonds were established between the residue H193 and carboxylic acid group of SAG. In the case of SghA–salicin, salicin orientation was similar to SAG, and structural comparison revealed that there was little change of the active site except for H193. H193 appeared to form a hydrogen bond with the hydroxymethyl group of salicinaglycone; however, its geometrical preference was less perfect than SghA–SAG.

In contrast to the compact and conserved bottom half of $(\beta/\alpha)_8$ barrel (β-strand N terminus side), the top half (β-strand C terminus side) of SghA was surrounded by 4 flexible loops that gate the exit of the bell-shaped cavity. It was proposed that these loops are involved in the formation of the aglycone-binding site that determines substrate preference (14). In particular, loops B and C of the 4 loops A to D (Fig. 2 *C* and *D*) are mainly responsible for aglycone binding. In line with this notion, residues H193 and W340, respectively, located in loop B and C established direct interactions with the SAG salicylic acid group or salicin. Residue W340 formed an imperfect π–π interaction with the benzene ring, considering that W340 is quite conserved in the binding pocket among SghA homologs whereas H193 is only found in the binding pocket of SghA (*SI Appendix*, Fig. S9). The unique residue H193 in agrobacterial SghA interacting with SAG only suggests that H193 might play a more crucial role in substrate recognition of SghA than other residues. H193 made strong hydrogen-binding interactions with the SAG salicylic acid group that rationalizes our biochemical data about the substrate preference of SghA to SAG, rather than salicin.

Compared with the structure of *Neotermes koshunensis* β-glucosidase (13), SghA exhibits a conserved substrate-binding site (*SI Appendix*, Fig. S9). It is common for GH1 family proteins to have subtle differences in substrate specificity. In addition to the native substrate, these proteins could hydrolyze a broad spectrum of artificial substrates. Similarly, SghA hydrolyzed ONPG and X-gal, which are synthetic analogs of SAG. The GH1 protein family hydrolyzes glycosidic bonds through a retention mechanism that retains the overall anomeric configuration of the saccharide substrate. The combined data of structural and biochemical analysis proposed that a catalytic mechanism of SghA on substrate SAG:E367 makes a nucleophilic attack on the anomeric carbon C1 in SAG and E179 acts as a proton donor to release SA (*SI Appendix*, Fig. S10).

SghR Suppresses *sghA* Expression by Binding to Its Promoter. Results of RT-PCR and real time RT-PCR analyses revealed that the level of *sghA* messenger RNA (mRNA) was much higher in *sghR* mutant than wild-type strain A6 at different intervals (Fig. 3*A* and *SI Appendix*, Fig. S11). Gel shift analysis showed that SghR directly and specifically bound with the *sghA* promoter to shift it in a dosage-dependent manner, but the control promoter (*pa0305* from *P. aeruginosa* PAO1) was unaffected by SghR (Fig. 3*B*). An unrelated IclR-type regulator (AttJ or BIcR) of *A. tumefaciens* also failed to shift the *sghA* promoter (15). Taken together, these results indicate that SghR suppresses *sghA* transcription via direct binding to its promoter in *A. tumefaciens*.

Sucrose Inactivates SghR and Induces *sghA* Expression. Given that SghA is tightly suppressed by SghR under in vitro conditions, we hypothesized that there might be a signal ligand interacting with SghR to induce *sghA* expression *in planta*. An extract of carrot

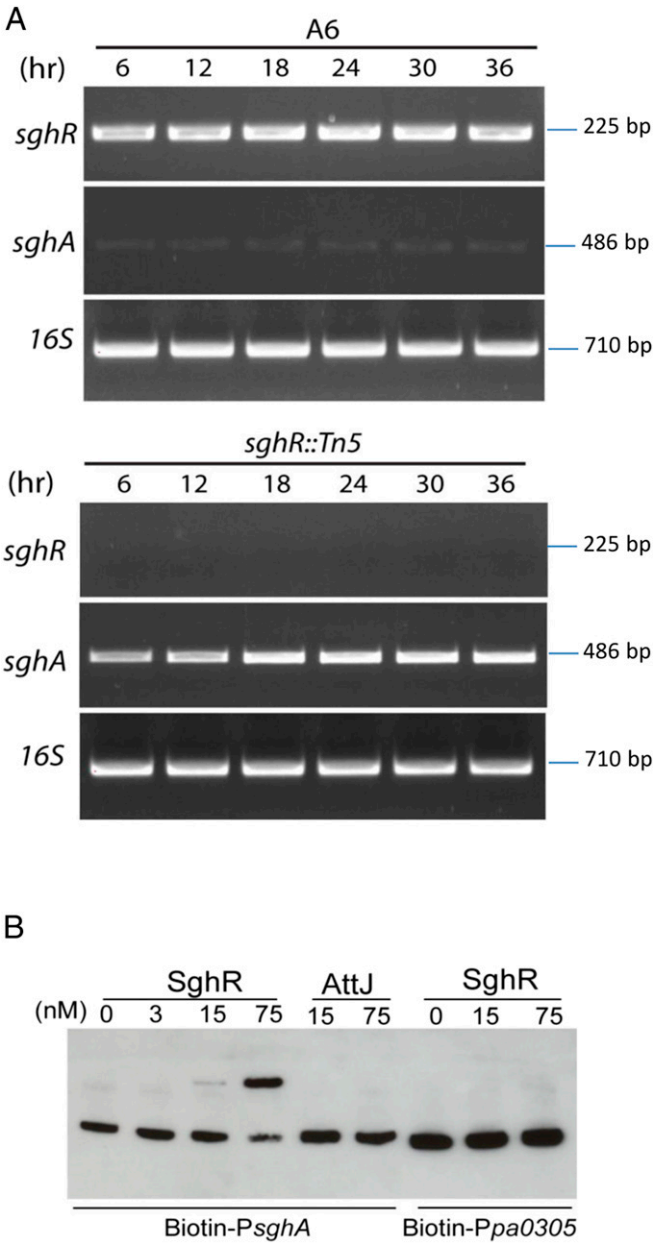

Fig. 3. SghR controls the transcriptional expression of *sghA*. (*A*) RT-PCR analysis of the *sghA* expression patterns in wild-type strain A6 and its *sghR* mutant at different time intervals postinoculation in BM medium with mannitol as the sole carbon source. (*B*) Electrophoretic mobility-shift assay (EMSA) analysis of SghR binding to the *sghA* promoter. The unrelated transcriptional regulator AttJ from *A. tumefaciens* and the promoter P*pa0305* from *P. aeruginosa* were used as specificity controls. Purified proteins of SghR and AttJ were mixed with the biotin-labeled probes (1 nM) at various concentrations, and reaction mixtures were separated by electrophoresis. Experiments were repeated at least 3 times with similar results, and 1 set of representative data is presented.

tubers was prepared to test its activity in the induction of β-galactosidase encoded by *sghA*, and results depicted that *sghA* expression was induced with the addition of the extract (Fig. 4*A*). To purify the active signal, dry powders of carrot extract were further extracted with methanol, and samples were separated by silica column chromatography. Active fractions were pooled, and a compound was crystallized during the evaporation of solvent. This crystallized molecule displayed a strong activity to induce *sghA* expression when dissolved in water (*SI Appendix*, Fig. S12*A*). MS analysis showed that the molecular weight of this compound is 342.20, and, together with the results of NMR analysis, the active compound was identified as disaccharide sucrose (*SI Appendix*, Fig. S12 *B–F*). Commercial sucrose induced β-galactosidase activity in *A. tumefaciens* A6 on the X-gal plate (Fig. 4*B*). Consistent with the above results, gel shift analysis demonstrated that sucrose dissociated repressor SghR from the *sghA* promoter. SghR binding to the *sghA* promoter was substantially reduced and completely abolished when sucrose was added at a final concentration of 50 μM and 500 μM, respectively (Fig. 4*C*). This is within the range of extracellular sucrose concentration *in planta*. Quantitative measurement of intercellular sucrose levels in carrot tissues showed that sucrose concentrations were higher than 40 mM in both uninoculated control and tissues infected with bacterial cells after deletion of *sghA* and *sghR* (*SI Appendix*, Fig. S13). These findings demonstrate that plant metabolite sucrose is a cognate signal deactivating SghR and induces transcriptional expression of *sghA*.

SghA Increases Plant SA Level during *A. tumefaciens* Infection. To confirm that SghA hydrolyzes SAG to SA during agrobacteria plant interaction, the level of free SA in infected plants was determined by using SA biosensor *Acinetobacter* sp. strain ADPWH_lux (16). Results revealed that inoculation of *sghR* mutant significantly enhanced free SA concentration in *Arabidopsis* at 20 h postinfection. Contrarily, challenge of the *sghA*/*sghR* double mutant led to lower SA level than plants inoculated with wild-type strain A6 (Fig. 5*A*). As expected, overexpression of *sghA* in the mutant *sghA::Tn5* resulted in substantially increased free SA level. Similar results were also obtained with HPLC by directly measuring free SA concentration in the roots of *Arabidopsis* infected with *A. tumefaciens* A6 and its derivatives (Fig. 5*B*). Data indicated that, during infection, *A. tumefaciens* used SghA to release SA from SAG in the host plant.

The tumor mass on *Arabidopsis* stems was measured to examine the impact of SghA-mediated SA increment in the host plant on bacterial infection (17, 18). Results showed that the tumor mass was substantially reduced in wild-type *Arabidopsis* ecotype WS-2 plants inoculated with the *sghR* mutant, as compared to those inoculated with wild-type *A. tumefaciens* A6. In contrast, disruption of *sghA* from the *sghR* mutant background led to significantly enhanced tumor growth, and tumor weight was almost 2 times that resulting from strain A6. Consistent with this trend, overexpression of *sghA* substantially attenuated bacterial tumorigenicity (Fig. 5*C*). These results were further consolidated by examining tumor weights on carrot discs (*SI Appendix*, Fig. S14*A*) and validated by quantification of tumor numbers after inoculation of carrot discs with serial dilutions of bacterial inoculum (*SI Appendix*, Fig. S14*B*).

Tumorigenicity of strain A6 and its derivatives was tested on *Arabidopsis* Ugt74f1 as control. *Arabidopsis* Ugt74f1 is a mutant derived from the *Arabidopsis thaliana* ecotype WS-2. In this mutant, SA glucosyltransferase was mutated to substantially reduce SAG formation, leading to a significantly higher SA level than in wild-type *Arabidopsis* (19, 20). As shown in Fig. 5*D*, strain A6 and its mutants caused a similar level of tumor growth on *Arabidopsis* Ugtf741, but the tumor mass was substantially less than that incited by strain A6 on wild-type *Arabidopsis*. In controls, no significant growth difference was recorded among wild-type and mutants in lysogeny broth (LB) and BM media, or with glucose and sucrose as the sole carbon source (*SI Appendix*, Fig. S15 *A–D*). *sghR*- and

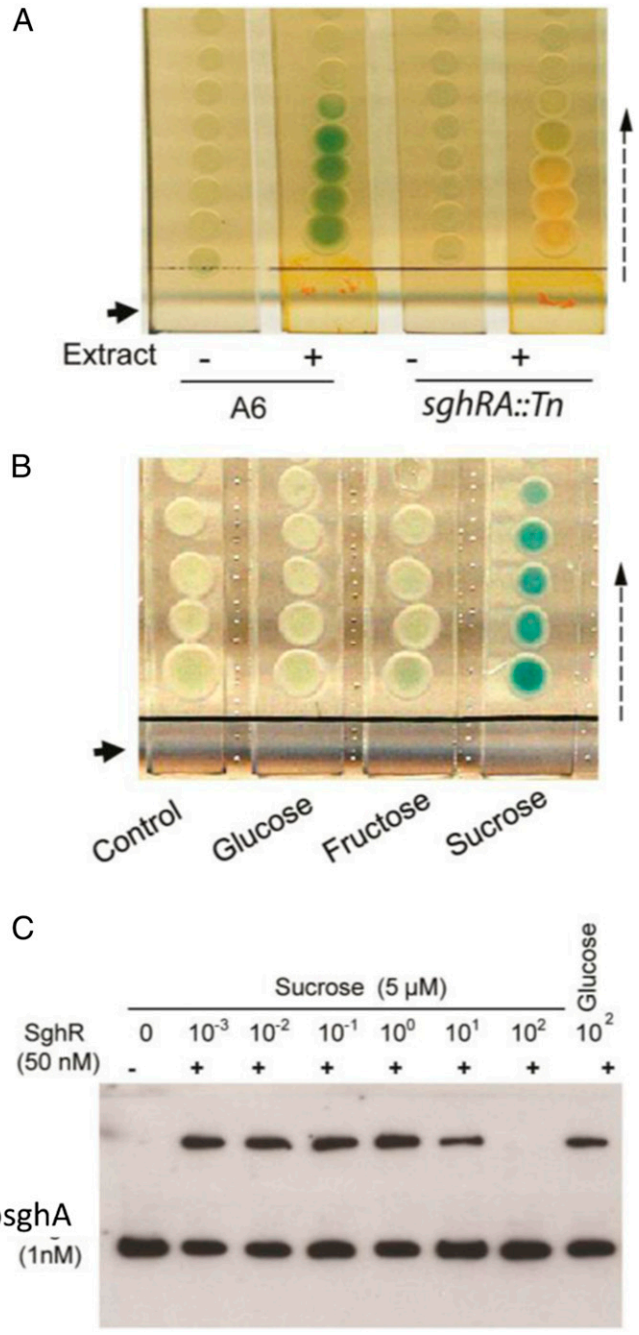

Fig. 4. Sucrose is the host signal that induces *sghA* expression. (*A*) X-gal plate assay of strain A6 *sghA*-encoded β-galactosidase activity in the presence or absence of carrot extract. A6, wild-type *A. tumefaciens* A6; sghRA::Tn, negative control of *A. tumefaciens* A6 with mutations in SghA and SghR. (*B*) Sucrose induced the expression of *sghA* in A6 on solid plates containing X-gal where *A. tumefaciens* A6 was spotted as the indictor strain on separated agar slices. The solid arrow in *A* and *B* represents the loading location of carrot extract and related compounds (5 μL of solution with a concentration of 1 M) on separated BM agar slices. The dashed arrow indicates the diffusion direction of the compounds. (*C*) EMSA analysis of sucrose activity in dissociation of SghR-promoter (P*sghA*) complex. Experiments were repeated at least 3 times with similar results, and 1 set of representative data is presented.

sghA-mutants produced similar levels of biofilms, and mRNA levels of *virE3* in mutants were comparable with wild-type strain A6 in virulence-inducible or noninducible media (*SI Appendix*, Fig. S15 *E* and *F*). Data are consistent with the notion that an

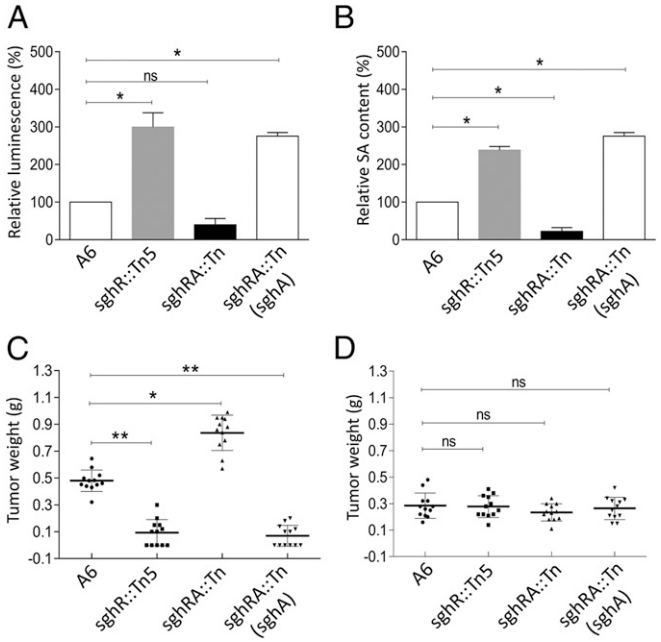

Fig. 5. SghA releases SA from SAG during bacterial infection and is involved in the modulation of tumor development. Biosensor analysis (*A*) and HPLC analysis (*B*) of SA in *Arabidopsis* roots infected with *A. tumefaciens* strain A6 and its derivatives. Experiments were repeated 5 times in duplicate, and relative fold change was calculated by normalizing against wild-type A6, arbitrarily set as 100%. (*C*) Tumor sizes incited by strain A6 and derivatives in *A. thaliana* wild-type Wassilewskija. (*D*) Tumor sizes incited by strain A6 and derivatives in the SAG-defective mutant of *A. thaliana* Ugt74f1. Experiments in *C* and *D* were repeated 3 times, and each time with 4 plants. Statistical analyses were performed with a nonparametric Kruskal–Wallis 1-way ANOVA test in GraphPad. Values and error bars represent means and SD. $*P < 0.05$; $**P < 0.001$; ns, not significant.

enhanced free SA level in host plants is positively associated with increased disease resistance and SghR/SghA play an important role in the modulation of *A. tumefaciens* virulence.

SghA-Released SA Reprograms *A. tumefaciens* Virulence. To understand the role of SghR/SghA in *A. tumefaciens* tumorigenicity, SA and SAG effects on the expression patterns of *sgh* and *vir* genes were analyzed. With a basal level of gene expression of *virE3* in BM minimal medium, real time RT-PCR results showed that SA and SAG treatments had no detectable effect on the expression of *sghR* and *sghA* in the presence or absence of functional SghA (*SI Appendix*, Fig. S16). SA significantly inhibited *virA* expression in all tested strains whereas SAG affected *virA* expression only in the presence of functional SghA (Fig. 6*A*). Results suggest an essential role of SghA in the modulation of *vir* gene expression by releasing SA from the inactive SAG.

RT-PCR and real-time RT-PCR were used to determine *in planta* expression patterns of *sgh* and *vir* genes in wild-type strain A6 at different intervals after the inoculation of *A. thaliana*. *SghA* and *vir* genes displayed differentially overlapping expression patterns while *sghR* constitutively expressed at different post-inoculation intervals (Fig. 6*B* and *SI Appendix*, Fig. S17). The 3 tested *vir* genes including *virA*, *virD2*, and *virE3* significantly expressed during early stages of infection at 6, 12, and 18 h post-inoculation, but their expressions were inhibited at the later stages. In contrast, hardly any *sghA* transcript was found at 6 and 12 h, and maximum expression occurred at 24 h postinoculation. Western blot analysis also showed that VirD2 protein expression in wild-type strain A6 occurred at around 12 h postinoculation, peaked at 24 h, and decreased afterward (Fig. 6*C*). Contrarily, *sghR* mutant resulted in a significantly decreased level of VirD2 protein (Fig. 6*C*), but *sghA* mutant caused higher expressions of VirD2, even at the later stage of infection. Taken together, these results suggest that SghR/SghA-mediated release of SA plays a key role in reprograming the virulence gene expression in *A. tumefaciens*.

Discussion

At least 2 lines of evidence indicate that the time required for tumor induction by *A. tumefaciens* is less than 10 h (21, 22), but expression patterns of the bacterial virulence gene after establishing infections is not clear. This study showed that, upon inoculation, *vir* genes of *A. tumefaciens* maintained a high level of expression *in planta* at the early stage of infection but their transcript levels were substantially decreased after 18 h. The key mechanism that reprograms *vir* gene expression in *A. tumefaciens* consists of a regulator and enzyme pair SghR/SghA that timely releases SA from SAG in a working model, as presented in Fig. 7. In this model, we proposed that plant SAG enters in agrobacterial cells for hydrolysis rather than the secretion of bacterial SghA to act extracellularly. Secretion-specific signal peptide was not identified in the SghA amino acid sequence; however, it is well-known that SAG analogs having high structural similarity with X-gal, ONPG, and salicin can enter bacterial cells. However, further studies using isotope-labeled SAG are required to verify this working model. SAG has been reported to exclusively deposit in the vacuole via ATP-dependent transportation (23), but it is currently unknown whether plant cells can also actively export SAG for hydrolysis. Generally, agrobacteria initiate infection at the wound site of the host plant, and SAG could be one of the wound-released chemical signals perceived by bacterial cells.

SghA is known to hydrolyze different compounds, such as X-gal, ONPG, and salicin. Biochemical and structural analyses in this study suggested that SAG can serve as a bona fide substrate of SghA because 1) SghA failed to hydrolyze coniferin and its inducer sucrose, 2) SghA mutant grows readily with sucrose as the only carbon source, and 3) SghA releases SA from SAG in a highly efficient manner, as compared to other substrates. SA is a key signal that activates both local and systemic acquired resistance to regulate disease resistance. Under normal growth conditions, SA conjugates with β-glucosides and is stored in the inactive form to minimize its cytotoxicity, maximize SA stability, and facilitate its transportation. Among SA conjugates, SAG has been identified as a predominant and stable metabolite (24, 25). A previous study showed that plant growth hormone auxin influences *A. tumefaciens* virulence by inhibiting *vir* gene induction and bacterial growth (26). However, this effect was only observed at higher concentrations of auxin (25 to 250 μM), marginally matching with its level in *Arabidopsis* crown galls (17.3 ± 8.8 μM) and taking multiple days from agrobacteria inoculation to the formation of visible crown galls (27). During this study, inactivation of SghA promoted tumor formation in plants whereas it failed to improve agrobacterial growth in vitro. Future work is required to examine whether specific release of SA from SAG by SghA benefits bacteria during in vivo infection. SA is considered a systemic signal triggering a defense response in uninfected host cells. Initiation of SA synthesis in host cells by SghA lacking pathogens suggests that SghA-based SA release is not the only mechanism to manipulate the host SA signaling pathway during microbial infection. SghA may also metabolize additional substrates, and the fact that SghA releases SA might be coincidental although it exhibits no enzymatic activity toward sucrose and coniferin.

Transcriptional repressor SghR and its cognate signal ligand sucrose control the expression of *sghA*. Mutation of *sghR* led to constitutional expression of *sghA*, suggesting that SghR is the key regulator that governs transcriptional expression of *sghA*. Our data revealed that *sghA* is specifically induced by the plant metabolite sucrose, which interacts to inactivate repressor SghR at a concentration lower than 0.5 mM. Sucrose is a major photosynthesis

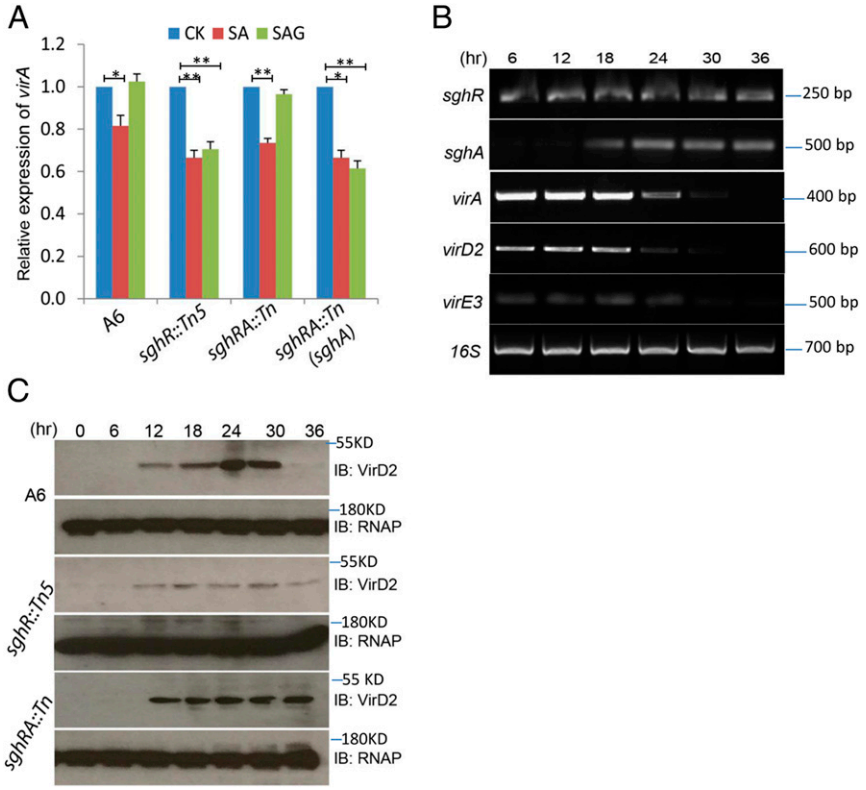

Fig. 6. SghA-releasing SA down-regulates *vir* gene expression of *A. tumefaciens* during plant infection. (*A*) Real time RT-PCR analysis of *virA* expression in the presence of SA and SAG, respectively. The *virA* expression level in blank control without treatment (CK) was arbitrarily set as 1. The error bar denotes the SD of 3 repeats. Experiments were repeated 3 times in duplicate. Statistical analyses were performed with a nonparametric 1-way ANOVA test in GraphPad. *significant < 0.05; **significant < 0.01; ns, not significant. (*B*) *In planta* expression patterns of *sgh* and *vir* genes of *A. tumefaciens* strain A6. The 16S rRNA was amplified as an internal control. (*C*) Western blot analysis of VirD2 *in planta* expression patterns using VirD-specific antibody. Expression levels of bacterial RNA polymerase (RNAP) were determined with beta subunit RNAP-specific antibody as a loading control. IB, immunoblot. KD, kilodalton.

product (>95%) in plants that could reach to a concentration of 1 M in conducting vascular cells and 2 to ∼7 mM in extracellular spaces (28). Consistent with this report, soluble sucrose concentration in carrot tissues was noted in the range of 47 to 100 mM, depending on postinoculation intervals. Extracellular concentration of sucrose can dramatically increase after tissue disruption. In addition to a carbon source, sucrose also acts as a signal molecule to regulate plant growth, development, differential gene expression, and stress-related responses (29). Furthermore, evidence supporting sucrose as a potent signal to induce plant defense responses has been reported (30, 31). However, the precise mechanism of sucrose-induced immunity and the related signaling pathway remains a mystery. Results of this study depict that sucrose specifically induces the expression of hydrolase SghA by deactivating repressor SghR, which degrades the SAG conjugate to increase the cellular level of plant signal SA. Therefore, identification of SghR/SghA depicts a mechanism that corroborates sucrose-induced immunity and explains that the SA level in plant tissues is not elevated by the initiation of agrobacterial infection, but dramatically enhances at the later infection stage (32).

Characterization of SghR/SghA unveils a mechanism that allows the bacterial pathogen to tap on the reserved pool of plant defense signal SA to reprogram its virulence gene expression after establishing infection. Bioinformatics analysis showed that SghA is highly conserved in *A. tumefaciens* and other members of the *Rhizobiaceae* family of α-proteobacteria. SghA shares moderate similarities with the homologs of other bacterial species, such as *Dickeya* and *Pectobacterium*. It is not clear whether these homologs can hydrolyze SAG or pair with an SghR-like regulator to release SA in a controlled manner. In this regard, it is interesting to note that SA could directly influence virulence gene expression in *A. tumefaciens* and other bacterial pathogens. At lower concentrations, SA was found to impair bacterial attachment and biofilm formation and down-regulate fitness and production of virulence factor in *P. aeruginosa* (33). Similarly, SA inhibited biofilm formation, motility, and *N*-acyl homoserine lactone quorum sensing signal production in *Pectobacterium carotovorum* and *Pseudomonas syringae* pv. *Syringae* (34). Moreover, the amazing sensing abilities of microbes and the response to changing environmental conditions require further investigations to unveil mechanisms that allow pathogens to reprogram virulence gene expression after establishing infections.

Methods

Bacterial Strains, Plasmids, and Growth Conditions. *SI Appendix*, Table S1 lists bacterial strains and plasmids used in this study. *A. tumefaciens* strains were grown at 28 °C in BM medium (pH 7.0, 0.2% mannitol) or in VIB medium (NH_4Cl, 1 g/L; $MgSO_4 \bullet 7H_20$, 0.3 g/L; KCl, 0.15 g/L; $CaCl_2$, 0.01 g/L; $FeSO_4 \bullet 7H_20$, 2.5 mg/L; K_2HPO_4, 0.06 g/L; NaH_2PO_4, 0.023 g/L; pH 5.5, 0.2% arabinose and 100 μM acetosyringone) (10). One liter of BM medium contained K_2HPO_4 (10.5 g), KH_2PO_4 (4.5 g), $MgSO_4 \bullet 7H_2O$ (0.2 g), $(NH_4)_2SO_4$ (2.0 g), $FeSO_4$ (5 mg), $CaCl_2$ (10 mg), $MnCl_2$ (2 mg), and mannitol (2.0 g). LB medium was used for general cultivation of *Escherichia coli* strains, and antibiotics were added at the following concentrations when required: kanamycin, 100 μg/mL; tetracycline, 5 μg/mL; gentamycin, 100 μg/mL; ampicillin, 200 μg/mL.

Genetic Manipulation of *A. tumefaciens*. Transposon mutagenesis was performed in *E. coli* BW020767 containing a mini Tn*5* or *E. coli* SM10 (pBT20) carrying a mariner transposon, and disrupted genes were identified (35). *A. tumefaciens* mutants were screened on BM solid plates containing X-gal (50 μg/mL) and relevant antibiotics. To conduct complementation analysis, a DNA fragment containing the putative promoter and full-length *sghA* was amplified from

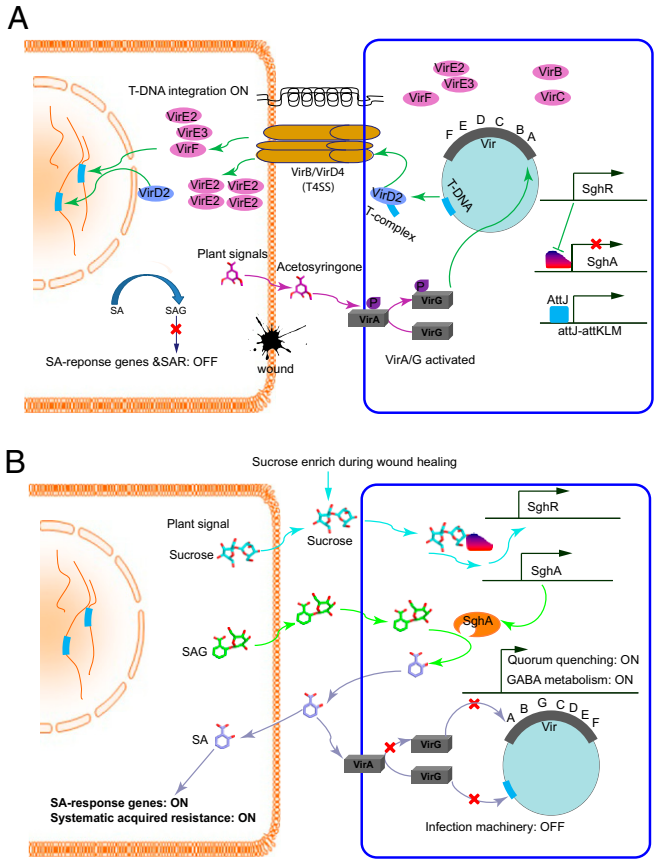

Fig. 7. Schematic presentation of entry and exit of *A. tumefaciens* infection. (*A*) Infection entry at the beginning of bacterial infection. The plant signal acetosyringone is released upon wounds to bind with sensor VirA and thereby activates VirG by phosphorylation. Activated VirG triggers *vir* gene expression and initiates T-DNA synthesis in *A. tumefaciens*. Bacterial type IV secretion system (T4SS) transfers T-DNA into plant cells and integrates into the plant chromosome. At this stage, salicylic acid (SA) is inactivated by conjugation with glucose to produce SAG in plant cells, SA-responsive genes are not induced, and genes encoding systematic acquired resistance (SAR) are turned off. In the bacterial cell, quorum quenching gene *attM* and SA hydrolase gene *sghA* are suppressed by AttJ and SghR, respectively. (*B*) Infection exit at the later stage of infection. Sucrose enhances at the wounded site during healing and is transported into bacterial cells to dissociate SghR from its complex with the promoter DNA inducing *sghA* expression. Accumulated SghA hydrolyzes SAG to release SA, which, on one hand, triggers the expression of the AttJ-AttKLM operon, thus initiating quorum quenching and γ-aminobutyric acid (GABA) catabolism systems inside the bacterial cells. On the other hand, released SA inactivates VirA to shut down infection machinery. Additionally, released SA could also activate plant SA responsive genes and SAR.

A. tumefaciens A6 by using PCR primers (*SI Appendix*, Table S2). The PCR product was digested by BamHI and cloned in pLAFR3, and the resultant construct pLA-*sghA* was verified by sequencing before transformation into *A. tumefaciens* by electroporation (15). Deletion of SghR, SghA, and its double deletion were performed according to Wang et al. (36).

Recombinant Proteins. The coding regions of target genes were amplified from the genomic DNA of *A. tumefaciens* A6 and fused into 6×His-tagged expression vector pET14b (Novagen). After verification by DNA sequencing, resultant constructs were separately transformed into strain BL21(DE3), and recombinant proteins were purified (37).

Enzyme Assay. SghA β-galactosidase activity was indicated by the appearance of a blue color on BM agar plates supplemented with X-gal (50 μg/mL) according to Zhang et al. (38). Briefly, solidified BM medium in Petri dishes was cut into separate slices, and plant extracts or chemical compounds were loaded at the end of the agar slice, which generated gradient concentrations of the tested sample by diffusing along the separated agar slices. Specified bacterial cultures were progressively spotted along the agar slice, and results were recorded after incubation at 28 °C for 48 h.

Quantification of β-galactosidase activity was carried out by gently shaking at 37 °C for 3 h in Z buffer (60 mM Na_2HPO_4, 40 mM NaH_2PO_4, 10 mM KCl, 1 mM $MgSO_4$, 50 mM β-ME, pH 7.0) containing 1 mM ONPG or salicin or SAG and 10 mM SghA. The same amount of boiled SghA was added to the reaction mixture as a negative control. Samples were introduced onto a symmetry reverse-phase column (4.6 × 250 mm) for HPLC. Fractions were eluted with 50/50 methanol/water (vol/vol) at a flow rate of 1 mL/min and detected by a Waters 996 photodiode detector. ESI-MS was performed on a Finnigan/MAT ion-trap mass spectrometer following standard procedures.

RT-PCR and Western Blot Analysis. To study *sghR* and *sghA* expression levels during bacterial growth, strain A6 and its mutant *sghR::Tn5* were cultivated in BM medium and harvested at specific time intervals. Total RNAs were extracted by using the RNeasy Mini Kit (Qiagen). To treat SAG and SA, specified bacterial cells were grown overnight in LB medium and then subcultured in 5 mL of induction medium (with 100 μM acetosyringone) at an initial OD600 of 0.1, with or without SAG (10 μM) and SA (5 μM). After 5 h of shaking (rpm 200) at 28 °C, 1 mL of cell cultures was harvested for RNA extraction with the RNAprotect Reagent Kit (Qiagen). Residual DNAs were digested by RNase-free DNase I (Promega), and its absence was validated by PCR with purified RNA templates. RNA integrity was assessed by agarose gel electrophoresis, and RNA concentration was measured by Nanodrop ND-1000 (Nanodrop Technologies). To minimize data variation, total RNAs were prepared from 3 independent repeats and pooled together for RT-PCR analysis.

The protocol of the 1-step strategy (Qiagen) was followed to conduct RT-PCR. An aliquot of 0.2 μg of total RNAs served as the template for RT-PCR to amplify a portion of target genes with primers (*SI Appendix*, Table S2). A fragment of 16S ribosomal RNA (rRNA) was also amplified in each RT-PCR as an internal control. An aliquot of 0.1 mg of total RNAs served as the template for real-time RT-PCR, and real-time reverse transcription-PCR analysis was performed in Rotor-Gene Q (Qiagen) by using the SYBR Green RT-PCR Kit (Qiagen). Housekeeping gene *rpoC* encoding the β subunit of RNA polymerase was included as an internal control. Results were presented as the ratio of target gene expression versus control gene. Real-time RT-PCR primers are listed in *SI Appendix*, Table S2.

To determine the expression levels of *sghR*, *sghA*, and *vir* genes during *Agrobacterium* infection, strain A6 cells grown in LB medium at late exponential phase were harvested, washed 3 times with DPBS (Dulbecco's phosphate-buffered saline) buffer and resuspended in the same buffer for carrot infection. Carrots were washed 3 times with 75% ethanol, sliced into 1.5-cm-thick disks, and inoculated with 200 μL of bacterial cells. Infected carrot disks were placed into Petri dishes moisturized with wet filter papers and incubated at 28 °C. Bacterial cells were collected at specific time intervals by washing with DPBS buffer containing Triton X-100 (0.1%), treated with RNAprotect Bacteria Reagent (Qiagen), and kept at −80 °C until RNA extraction. RT-PCR was conducted following the protocol of the 1-step strategy (Qiagen) or 2-step strategy (Promega). An aliquot of 0.2 μg of total RNAs was used as template to amplify a portion of the target genes with primers listed in *SI Appendix*, Table S2.

Western blotting was carried out by harvesting bacterial cells from infected plant tissues as mentioned above and lysed in urea buffer (100 mM NaH_2PO_4, 10 mM Tris·HCl, 8 M Urea, 1 mM Na_3VO_4, 20 mM NaF, 0.1 mM β-glycerophosphate, and 20 mM sodium pyrophosphate) supplemented with a complete Protease Inhibitor Mixture tablet (Roche, pH 8.0). Lysates were cleared by centrifugation (14,000 rpm, 10 min, 4 °C), and protein concentration in supernatants was determined with the BCA Protein Assay Kit (Pierce). Equal amounts of total proteins were used for Western blot with VirD2-specific (catalog no. MBS5304219; Mybiosource) and RNA polymerase (RNAP)-specific antibodies (catalog no. 663903; Biolegend,).

Electrophoretic Mobility-Shift Assay. The S*ghA* promoter region (−345 bp to +43 bp) was amplified from genomic DNA of *A. tumefaciens* strain A6 by using 5′-biotinylated primers (*SI Appendix*, Table S2). The fragment was designated as P*sghA* and used as a probe for gel retardation analysis to determine potential interaction with transcriptional repressor SghR. As a specificity control, PCR was used to generate the P*pa0305* probe (−281 bp to +81 bp) from genomic DNA of *P. aeruginosa* with 5′-biotinylated primers (*SI Appendix*, Table S2). A gel retardation assay was performed with the LightShift Chemiluminescent EMSA Kit by following the recommended protocol (Pierce Biotechnology).

SA Measurement. *A. thaliana* ecotype WS-2 seeds were sterilized with a solution (50% bleach and 0.1% SDS) for 10 min and rinsed in sterile water several times. Seeds were placed on MS agar plates (Sigma), incubated at 4 °C for 2 d, and transferred to a growth chamber with a short-day (8 h light) photoperiod at 23 °C for root culture. After 2 wk, roots were axenically cut into ~3-cm segments on a sterile filter paper and transferred to MS medium for agrobacterial infection. Root segments were collected at 20 h post-infection for SA extraction and quantified with HPLC (39) and biosensor *Acinetobacter* sp. ADPWH_lux (16).

Protein Preparation, Crystallization, and Structural Determination. The SghA coding region was amplified by PCR and cloned into vector pET-14b. The resultant construct was verified by DNA sequencing and transformed into *E. coli* BL21 CodonPlus-(DE3) RIL for protein expression. SghA purification was carried out according to Ye et al. (37). SghA derivative E179S was generated by QuikChange (Stratagene) and purified by following the same procedure as SghA.

Crystallization of SghA has been previously reported (37). To crystallize SghA–SAG, –salicin, and –glucose protein–ligand complexes, the ligands were mixed with SghA derivative E179S at a final concentration of 20 mM and incubated for 30 min at room temperature, followed by a similar crystallization procedure for the apo form.

Diffraction data were collected at 100 K on beam lines I04 (Diamond) or X06SA (Swiss Light Source). Data were processed in XDS (40), and structures were determined with Phaser (41) using homolog structure (PDB ID code 1NP2) as a search model for SghA. Automatic model building was performed in ARP/wARP (40) and improved by building a manual model with COOT (42). Models were refined with Phenix (43) and checked by PROCHECK (44). Crystallographic data and refinement statistics are listed in *SI Appendix*, Table S3, and figures were generated with Pymol (Delano Scientific).

Quantitative Analysis of Soluble Sucrose in Carrot Tissues. The overnight starter cultures of *A. tumefaciens* strains were inoculated (1%) in 20 mL of LB medium and grown at 28 °C and 200 rpm until OD_{600} reached to 1.0. Bacterial cells were collected by centrifuging at 12,000 rpm for 10 min, washed twice with sterile PBS buffer, and resuspended in 2 mL of the same buffer. Carrot samples were sterilized with 80% ethanol and dissected into 1-cm-thick slices. Each carrot slice was evenly spread with 100 μL of bacterial solution, placed on a Petri dish with moisturized filter papers, and incubated at 28 °C for 6 h. Similarly, PBS buffer was added to serve as a control. To measure extracellular sucrose concentration, carrot samples were collected and washed with sterile water to remove bacterial cells. Slices were dried with tissue paper, and a thin layer (2 mm) was cut from the end of inoculation and weighed. Apoplastic fluid was collected with an infiltration technique as previously described (45). After infiltration, carrots were centrifuged at 650 × *g* for 10 min at 4 °C. Intercellular sucrose content was then determined with sucrose assay kit SCA20-1KT (Sigma-Aldrich) by following the manufacturer's protocol. Carrot tissue powders were extracted 3 times with 1 mL of sterile water, mixed thoroughly, and placed in a 60 °C water bath for 15 min. Supernatants were collected by centrifuging for 10 min at 12,000 rpm. Supernatants of the same sample were combined, and sterile water was added to a final volume of 11 mL, which was diluted accordingly for sucrose quantification with the SCA20-1KT.

Tumorigenesis Assay. *Arabidopsis* infection was carried out according to Deeken et al. (46). Briefly, *A. thaliana* seeds were cultivated in a growth room under a short-day condition at 23 °C. Tumors were induced by applying *A. tumefaciens* strains to the base of a wounded young inflorescence stalk. Disease symptoms were recorded on the 28th day of infection. Statistical analyses were conducted with the nonparametric 1-way ANOVA test.

ACKNOWLEDGMENTS. We thank Dr. Hui Wang (Natural Environment Research Council/Centre for Ecology and Hydrology, Oxford) for providing *Acinetobacter* sp. strain ADPWH_lux, and Prof. John V. Dean (DePaul University) for critical comments on SA measurement and providing *Arabidopsis* seeds. We also thank T. Tomizaki and M. Wang (Swiss Light Source) for help in X-ray data collection. This work was supported by National Program on Key Basic Research Project (973 Program) of China 2015CB150600 and the Agency for Science, Technology and Research in Singapore (to L.-H.Z.), Nanyang Technological University Integrated Medical, Biological and Environmental Life Sciences Grant NIM/01/2018 (to Y.-G.G.), and Basic Scientific Research Project of Chongqing Science and Technology Commission CSTC2018JXJL0230 (to X.L.).

1. J. R. Zupan, P. Zambryski, Transfer of T-DNA from Agrobacterium to the plant cell. *Plant Physiol.* **107**, 1041–1047 (1995).
2. K. A. Coggan, M. C. Wolfgang, Global regulatory pathways and cross-talk control pseudomonas aeruginosa environmental lifestyle and virulence phenotype. *Curr. Issues Mol. Biol.* **14**, 47–70 (2012).
3. L. A. Knodler *et al.*, Dissemination of invasive Salmonella via bacterial-induced extrusion of mucosal epithelia. *Proc. Natl. Acad. Sci. U.S.A.* **107**, 17733–17738 (2010).
4. L. W. Moore, W. S. Chilton, M. L. Canfield, Diversity of opines and opine-catabolizing bacteria isolated from naturally occurring crown gall tumors. *Appl. Environ. Microbiol.* **63**, 201–207 (1997).
5. A. Brencic, S. C. Winans, Detection of and response to signals involved in host-microbe interactions by plant-associated bacteria. *Microbiol. Mol. Biol. Rev.* **69**, 155–194 (2005).
6. J. Schell *et al.*, Interactions and DNA transfer between Agrobacterium tumefaciens, the Ti-plasmid and the plant host. *Proc. R. Soc. Lond. B Biol. Sci.* **204**, 251–266 (1979).
7. E. W. Nester, Agrobacterium: Nature's genetic engineer. *Front. Plant Sci.* **5**, 730 (2015).
8. A. C. Braun, R. J. Mandle, Studies on the inactivation of the tumor-inducing principle in crown gall. *Growth* **12**, 255–269 (1948).
9. A. Anand *et al.*, Salicylic acid and systemic acquired resistance play a role in attenuating crown gall disease caused by Agrobacterium tumefaciens. *Plant Physiol.* **146**, 703–715 (2008).
10. Z. C. Yuan *et al.*, The plant signal salicylic acid shuts down expression of the vir regulon and activates quormone-quenching genes in Agrobacterium. *Proc. Natl. Acad. Sci. U.S.A.* **104**, 11790–11795 (2007).
11. Z. Chen, D. F. Klessig, Identification of a soluble salicylic acid-binding protein that may function in signal transduction in the plant disease-resistance response. *Proc. Natl. Acad. Sci. U.S.A.* **88**, 8179–8183 (1991).
12. N. Yalpani, I. Raskin, Salicylic acid: A systemic signal in induced plant disease resistance. *Trends Microbiol.* **1**, 88–92 (1993).
13. W. Y. Jeng *et al.*, High-resolution structures of Neotermes koshunensis β-glucosidase mutants provide insights into the catalytic mechanism and the synthesis of glucoconjugates. *Acta Crystallogr. D Biol. Crystallogr.* **68**, 829–838 (2012).
14. Y. Nijikken *et al.*, Crystal structure of intracellular family 1 beta-glucosidase BGL1A from the basidiomycete Phanerochaete chrysosporium. *FEBS Lett.* **581**, 1514–1520 (2007).
15. C. Wang, H. B. Zhang, L. H. Wang, L. H. Zhang, Succinic semialdehyde couples stress response to quorum-sensing signal decay in Agrobacterium tumefaciens. *Mol. Microbiol.* **62**, 45–56 (2006).
16. W. E. Huang *et al.*, Chromosomally located gene fusions constructed in Acinetobacter sp. ADP1 for the detection of salicylate. *Environ. Microbiol.* **7**, 1339–1348 (2005).
17. R. Chevrot *et al.*, GABA controls the level of quorum-sensing signal in Agrobacterium tumefaciens. *Proc. Natl. Acad. Sci. U.S.A.* **103**, 7460–7464 (2006).
18. E. Haudecoeur *et al.*, Proline antagonizes GABA-induced quenching of quorum-sensing in Agrobacterium tumefaciens. *Proc. Natl. Acad. Sci. U.S.A.* **106**, 14587–14592 (2009).
19. Y. Noutoshi *et al.*, Novel plant immune-priming compounds identified via high-throughput chemical screening target salicylic acid glucosyltransferases in Arabidopsis. *Plant Cell* **24**, 3795–3804 (2012).
20. J. V. Dean, S. P. Delaney, Metabolism of salicylic acid in wild-type, ugt74f1 and ugt74f2 glucosyltransferase mutants of Arabidopsis thaliana. *Physiol. Plant.* **132**, 417–425 (2008).
21. L. C. Sykes, A. G. Matthysse, Time required for tumor induction by Agrobacterium tumefaciens. *Appl. Environ. Microbiol.* **52**, 597–598 (1986).
22. E. L. Virts, S. B. Gelvin, Analysis of transfer of tumor-inducing plasmids from Agrobacterium tumefaciens to Petunia protoplasts. *J. Bacteriol.* **162**, 1030–1038 (1985).
23. J. V. Dean, J. D. Mills, Uptake of salicylic acid 2-O-beta-D-glucose into soybean tonoplast vesicles by an ATP-binding cassette transporter-type mechanism. *Physiol. Plant.* **120**, 603–612 (2004).
24. H. I. Lee, I. Raskin, Glucosylation of salicylic acid in Nicotiana tabacum Cv. Xanthi-nc. *Phytopathology* **88**, 692–697 (1998).
25. P. Silverman *et al.*, Salicylic acid in rice (biosynthesis, conjugation, and possible role). *Plant Physiol.* **108**, 633–639 (1995).
26. P. Liu, E. W. Nester, Indoleacetic acid, a product of transferred DNA, inhibits vir gene expression and growth of Agrobacterium tumefaciens C58. *Proc. Natl. Acad. Sci. U.S.A.* **103**, 4658–4662 (2006).
27. J. Gohlke, R. Deeken, Plant responses to Agrobacterium tumefaciens and crown gall development. *Front. Plant Sci.* **5**, 155 (2014).
28. K. Koch, Sucrose metabolism: Regulatory mechanisms and pivotal roles in sugar sensing and plant development. *Curr. Opin. Plant Biol.* **7**, 235–246 (2004).
29. J. Wind, S. Smeekens, J. Hanson, Sucrose: Metabolite and signaling molecule. *Phytochemistry* **71**, 1610–1614 (2010).
30. M. R. Bolouri Moghaddam, W. Van den Ende, Sugars and plant innate immunity. *J. Exp. Bot.* **63**, 3989–3998 (2012).
31. J. Hanson, S. Smeekens, Sugar perception and signaling–An update. *Curr. Opin. Plant Biol.* **12**, 562–567 (2009).
32. C. W. Lee *et al.*, Agrobacterium tumefaciens promotes tumor induction by modulating pathogen defense in Arabidopsis thaliana. *Plant Cell* **21**, 2948–2962 (2009).
33. B. Prithiviraj *et al.*, Down regulation of virulence factors of Pseudomonas aeruginosa by salicylic acid attenuates its virulence on Arabidopsis thaliana and Caenorhabditis elegans. *Infect. Immun.* **73**, 5319–5328 (2005).
34. L. Lagonenko, A. Lagonenko, A. Evtushenkov, Impact of salicylic acid on biofilm formation by plant pathogenic bacteria. *J. Biol. Earth Sci.* **3**, 6 (2013).
35. R. A. Larsen, M. M. Wilson, A. M. Guss, W. W. Metcalf, Genetic analysis of pigment biosynthesis in Xanthobacter autotrophicus Py2 using a new, highly efficient transposon mutagenesis system that is functional in a wide variety of bacteria. *Arch. Microbiol.* **178**, 193–201 (2002).

36. C. Wang, D. Tang, Y. G. Gao, L. H. Zhang, Succinic semialdehyde promotes prosurvival capability of Agrobacterium tumefaciens. *J. Bacteriol.* **198**, 930–940 (2016).
37. F. Ye, C. Wang, Q. Fu, L. H. Zhang, Y. G. Gao, Cloning, expression, purification and crystallization of a pair of novel virulence factors, SghA and SghR, from Agrobacterium tumefaciens. *Acta Crystallogr. F Struct. Biol. Commun.* **71**, 1139–1145 (2015).
38. H. B. Zhang, L. H. Wang, L. H. Zhang, Genetic control of quorum-sensing signal turnover in Agrobacterium tumefaciens. *Proc. Natl. Acad. Sci. U.S.A.* **99**, 4638–4643 (2002).
39. Y. M. Gaspar *et al*., Characterization of the Arabidopsis lysine-rich arabinogalactan-protein AtAGP17 mutant (rat1) that results in a decreased efficiency of agrobacterium transformation. *Plant Physiol.* **135**, 2162–2171 (2004).
40. G. Langer, S. X. Cohen, V. S. Lamzin, A. Perrakis, Automated macromolecular model building for X-ray crystallography using ARP/wARP version 7. *Nat. Protoc.* **3**, 1171–1179 (2008).
41. A. J. McCoy, Solving structures of protein complexes by molecular replacement with Phaser. *Acta Crystallogr. D Biol. Crystallogr.* **63**, 32–41 (2007).
42. P. Emsley, B. Lohkamp, W. G. Scott, K. Cowtan, Features and development of Coot. *Acta Crystallogr. D Biol. Crystallogr.* **66**, 486–501 (2010).
43. P. V. Afonine *et al*., Towards automated crystallographic structure refinement with phenix.refine. *Acta Crystallogr. D Biol. Crystallogr.* **68**, 352–367 (2012).
44. R. A. Laskowski, J. A. Rullmannn, M. W. MacArthur, R. Kaptein, J. M. Thornton, AQUA and PROCHECK-NMR: Programs for checking the quality of protein structures solved by NMR. *J. Biomol. NMR* **8**, 477–486 (1996).
45. G. Lohaus *et al*., Solute balance of a maize (Zea mays L.) source leaf as affected by salt treatment with special emphasis on phloem retranslocation and ion leaching. *J. Exp. Bot.* **51**, 1721–1732 (2000).
46. R. Deeken *et al*., Tumour development in Arabidopsis thaliana involves the Shaker-like K+ channels AKT1 and AKT2/3. *Plant J.* **34**, 778–787 (2003).